Self-propelled hard disks: implicit alignment and transition to collective motion

Khanh-Dang Nguyen Thu Lam, Michael Schindler, Olivier Dauchot

UMR Gulliver 7083 CNRS, ESPCI ParisTech, PSL Research University,
10 rue Vauquelin, 75005 Paris, France

Abstract. We formulate a model of self-propelled hard disks whose dynamics is governed by mutually coupled vectors for velocity and body orientation. Numerical integration at low densities reveals that the expected transition from isotropic to aligned collective motion is present. However, the transition at the Landau mean-field level is strongly first-order, while it is continuous in the Vicsek model. We show that this difference is rooted in the complete opposite effect that individual scattering events have on alignment. We argue that such differences will generically hold for systems of self-propelled particles with repulsive short-ranged interactions. We obtain these results by matching the numerical results to the framework of Boltzmann theory, based on the statistics of binary scattering properties, always assuming that the system is small enough to stay homogeneous. We further show that the presence of noise in the dynamics can change the nature of the transition from discontinuous to continuous.

1. Introduction

Self-propelled particles borrow energy from their environment and convert it to translational motion. Depending on density and interaction details, energy taken up on the microscopic scale can be converted into macroscopic, collective motion – a transition from an isotropic phase to a polar, collective phase is observed. Most theoretical knowledge about such *active matter* and its transitions has been developed for Vicsek-like models: point particles travel at a speed which is constant to represent self-propulsion, and their direction changes according to interaction rules which comprise both explicit alignment and noise, to account for external or internal perturbations. In addition, self-diffusion noise may be incorporated in the individual motion. Typically, the alignment strength and noise intensity control the transition between the isotropic and the polar phases [1, 2, 3, 4, 5, 6].

In order to describe more closely experiments with bacteria [7, 8, 9] or with self-propelled actin filaments [10], other models incorporate explicitly the body-fixed axis of these particles. Also the alignment mechanism depends on this axis through the steric interaction of elongated objects [11, 12, 13]. The interaction thus uses both the velocity vector and the orientation axis of these particles, and is in some sense more explicit and *microscopic* than the purely effective (mesoscopic) alignment rules in Vicsek-like models. Alternatively, for circular or spherical particles, a natural way of producing alignment is to incorporate inelasticity or softness in the interaction rules [14, 15, 16, 17]. Not surprisingly, also these models exhibit a transition to a globally aligned phase.

We want to make further conceptual progress on how the microscopic interactions among self-propelled particles produce effective alignment. Are inelasticity or softness necessary ingredients? Or, – as suggested by observations of vibrated polar disks [18, 19] – does alignment come from re-collisions of particle pairs, between which their velocity vectors repeatedly converge towards each other? More generally, is it only the *interaction* between particles which enters the effective alignment, or also the individual *self-propelled motion* of particles between interactions? In the quest for answers, we want to start from firm grounds, where the interaction is that of elastic hard disks. Its contribution to "activeness", if any, is thus necessarily coupled with the dynamics. Also, as a first step, we shall focus on the mean-field level of description of the transition to collective motion, for which precise statements can be made regarding the connection between the effective alignment during scattering events and the phase transition at large scale.

In this paper, (i) we formulate a model of active liquid, made of self-propelled hard disks which interact through elastic collisions.‡ As we shall see, the key ingredient of the model is the *mutual* coupling of the positional and orientational degrees of freedom in the dynamics of each particle. We argue that this coupling is generically present in

‡ At first sight, the model might appear as a simplified version of the more ad-hoc one [20] used to reproduce and to interpolate numerically the vibrated polar disks experiment [18, 19]. However, we here present it starting from minimal principles using the mechanics of rigid bodies.

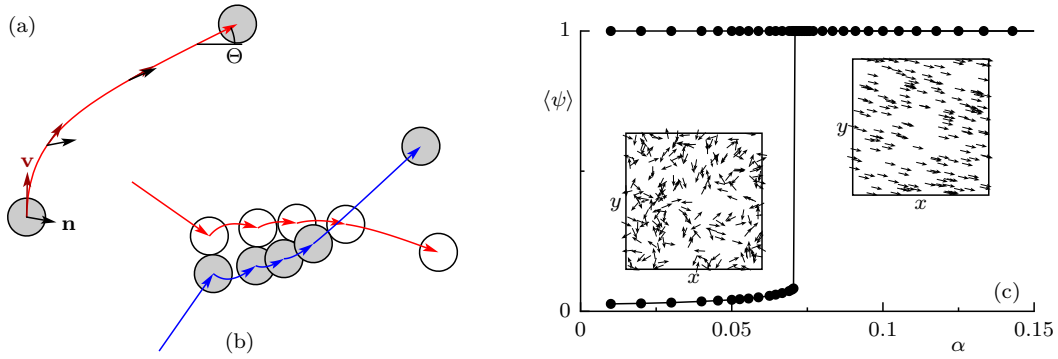

Figure 1. **(a)** An isolated self-propelled particle converges to its stationary state where velocity $\mathbf{v}$ and polarity $\hat{\mathbf{n}}$ are parallel. **(b)** A single binary "scattering event" can consist of many hard-disk elastic collisions. **(c)** Stable phases in the absence of noise. Between isotropic ($\langle\psi\rangle \approx 0$) and polar ($\langle\psi\rangle = 1$) phase is a discontinuous transition.

real systems of self-propelled particles, as soon as they are not point-like. The nature of the interaction itself is not essential. We chose it here to be hard core repulsion, and then compare with other models of self-propelled disks found in the literature. (ii) We integrate the model equations numerically, with and without noise. We focus on the transition between homogeneous phases which are theoretically tractable at the mean-field level. To do so, we restrict the simulations to "small" enough systems, such that the spatial inhomogeneities, which are frequently encountered in active systems, do not develop. We obtain the following phase diagram: in the absence of noise, the system exhibits a strongly first-order transition from the isotropic to the collective motion phase (see Fig. 1c). Above a finite level of noise, the transition turns second order at a tricritical point. (iii) We analyze the model equations on the grounds of a Boltzmann-like equation, by making use of a recently proposed observable $\langle \mathbf{p} \cdot \delta\mathbf{p} \rangle$ which quantifies the non-conservation of momentum [21]. This observable allows to span the bridge from the microscopic dynamics, in particular binary collisions such as depicted in Fig. 1b, to the Landau coefficients for the dynamics of the macroscopic order parameters. From direct sampling of all possible binary scattering events, we obtain an excellent quantitative prediction of our numerical findings. We thereby demonstrate that self-propelled hard disks generate effective alignment, provided that translational and orientational degrees of freedom are coupled to each other. Neither inelasticity nor softness are requested. Even the re-collisions alluded to in [18, 19, 20] are not necessary. (iv) We scrutinize the very peculiar dynamics of a single collision between two self propelled disks and explain the specific shape of the scattering function that was obtained numerically. In turn, this result explains how self-propulsion intrinsically generates effective alignment, requiring from the interaction only to be repulsive.

2. Model of self-propelled hard disks

The model consists of N hard disks in a square box of size $L \times L$, with periodic boundary conditions. The particles collide elastically when they touch, otherwise they follow a self-propelled motion without interacting.

2.1. Trajectories between collisions

A particle i is described by its center $\mathbf{r}_i(t)$, its velocity $\mathbf{v}_i(t)$, and by a unit vector $\hat{\mathbf{n}}_i(t)$ along its body axis, see Fig. 1a. We assume a self-propelling force $F_0\hat{\mathbf{n}}_i$ parallel to the body axis, and a dissipative force $\mathbf{F_D} = -\gamma\mathbf{v_i}$ parallel to and opposed to the velocity $\mathbf{v}_i$. The dissipation compensates the acceleration produced by the self-propelling force and allows a stationary speed of the individual particle.

In general, particle velocity $\mathbf{v}_i$ and particle axis $\hat{\mathbf{n}}_i$ are not aligned to each other. Then, the velocity has the tendency to align with the axis, because the acceleration due to self-propulsion is proportional to $\hat{\mathbf{n}}_i$. The viscous damping prevents the absolute value of the velocity from growing but has no influence on its direction. At the same time as $\mathbf{v}_i$ aligns to $\hat{\mathbf{n}}_i$, also the reverse is true, $\hat{\mathbf{n}}_i$ aligns to $\mathbf{v}_i$. This is the key ingredient of the model, and it is naturally motivated by the behaviour of any macroscopic rigid body: Imposing that the self-propulsion is not chiral, namely that the propulsion mechanism is mirror-symmetric with respect to the body axis $\hat{\mathbf{n}}_i$, as soon as $\mathbf{v}_i$ is not aligned with $\hat{\mathbf{n}}_i$, a torque acting on the particle is not forbidden by symmetry. A nonzero torque can therefore be considered the general case, and it will either turn $\hat{\mathbf{n}}_i$ towards $\mathbf{v}_i$, leading to a stable trajectory, or it will turn $\hat{\mathbf{n}}_i$ away from $\mathbf{v}_i$, thus destabilizing the trajectory. We here assume the first case, and simplify the equations by using an overdamped dynamics for $\hat{\mathbf{n}}_i$. The relaxation of $\hat{\mathbf{n}}_i$ towards $\mathbf{v}_i$ was a decisive ingredient when reproducing the experimental system of vibrated self-propelled disks [20]; it however applies more generally.

The mutual relaxation towards each other causes the two vectors to converge against a common stationary direction, where $\mathbf{v}_i = v_0\hat{\mathbf{n}}_i$. Here, $v_0 = F_0/\gamma$ denotes the final speed of the isolated particle. We choose the mass m of the particles, their diameter d_0, and d_0/v_0, as units of mass, length and time. The above arguments are then cast into the following dimensionless equations,

$$\frac{\mathrm{d}}{\mathrm{d}t}\mathbf{r}_i = \mathbf{v}_i, \tag{1}$$

$$\tau_v \frac{\mathrm{d}}{\mathrm{d}t}\mathbf{v}_i = \hat{\mathbf{n}}_i - \mathbf{v}_i + \sum_j \mathbf{f}_{ij}, \tag{2}$$

$$\tau_n \frac{\mathrm{d}}{\mathrm{d}t}\hat{\mathbf{n}}_i = (\hat{\mathbf{n}}_i \times \hat{\mathbf{v}}_i) \times \hat{\mathbf{n}}_i. \tag{3}$$

The interactions between particles, $\mathbf{f}_{ij}$ in Eq. (2) is discussed below, Sec. (2.2).

The two dimensionless parameters of the model are τ_n and $\tau_v = mF_0/\gamma^2 d$. In principle, when a particle starts with given $\mathbf{v}_i \neq \hat{\mathbf{n}}_i$, the trajectory depends on both

parameters τ_v and τ_n. It turns out, however, that the final direction of the particle depends on these parameters mostly through their ratio,§

$$\alpha = \frac{\tau_n}{\tau_v}, \tag{4}$$

which can be understood as the persistence of the polarity vector $\hat{\mathbf{n}}$. We therefore prefer this parameter when we discuss the overall behavior of the model in the sections below. The two extreme cases are already clear: When $\alpha \ll 1$, then $\hat{\mathbf{n}}$ aligns very fast and is practically always parallel to $\mathbf{v}$. Conversely when $\alpha \gg 1$, then $\hat{\mathbf{n}}$ dictates the orientation of $\mathbf{v}$. Quite remarkably, the experiments conducted with the vibrated polar disks seem to work in the crossover between these limits, $\alpha \simeq 1$ [20].

Finally, on top of the deterministic trajectories given by Eqs. (1)–(3), one can add some angular noise by the following procedure: When discretizing the dynamics with a given time step δt, we rotate $\mathbf{v}_i(t)$ and $\hat{\mathbf{n}}_i(t)$ by the same random angle $\eta_i(t)$, distributed normally with zero mean and variance $2D\delta t$.‖ The constant $D \geq 0$ fixes the level of the angular noise. Noises of different particles are statistically independent. We choose δt much smaller than the timescales in the dynamics, τ_v and τ_n. The relevant parameter to characterize the angular noise is then D/λ, where $\lambda = 4\rho/\pi$ is the characteristic scattering rate of the system, and is proportional to the density $\rho = N/L^2$ [21].

Note that the model is physically relevant in the absence of noise. Note further that setting the self-propulsion and the related damping to zero, Eq. (2) for the velocity decouples from Eq. (3) for the body vector, and one recovers the dynamics of an equilibrium hard disks liquid.

2.2. Particle collisions

The interactions between particles, $\mathbf{f}_{ij}$ in Eq. (2) are chosen as elastic hard-disk collisions: Particles 1 and 2 collide instantaneously, and their post-collisional variables are given in terms of their pre-collisional variables by

$$\begin{aligned} \mathbf{v}_1' &= \mathbf{v}_1 + J\,(\mathbf{r}_2 - \mathbf{r}_1), \qquad & \hat{\mathbf{n}}_1' &= \hat{\mathbf{n}}_1, \\ \mathbf{v}_2' &= \mathbf{v}_2 - J\,(\mathbf{r}_2 - \mathbf{r}_1), \qquad & \hat{\mathbf{n}}_2' &= \hat{\mathbf{n}}_2, \end{aligned} \tag{5}$$

where $J = (\mathbf{v}_2 - \mathbf{v}_1) \cdot (\mathbf{r}_2 - \mathbf{r}_1)$ quantifies the exchange of momentum between the two particles and is always negative when a collision occurs.

§ In the limit of small perturbation by the collision, we can linearize the evolution equations (1)–(3) around the stationary state. There, the final angle of the body axis is given *only* by the ratio α, namely as the weighted average of the initial angles θ_v and θ_n (the respective angles of $\mathbf{v}$ and $\hat{\mathbf{n}}$): $(\theta_v + \alpha\theta_n)/(1+\alpha)$.

‖ The initial motivation of this choice was to keep the multiple recollision dynamics rather unaffected by the action of the noise. As we shall see later, the recollisions are not an essential ingredient for the alignment – an unanticipated result – and the noise could have been implemented on the body axis $\hat{\mathbf{n}}$ only.

2.3. Scattering events

Equations (5) express the change of velocities while conserving momentum and energy. The polarities are left unchanged *by the collision*. After a collision, however, for both concerned particles $\mathbf{v}_i$ and $\hat{\mathbf{n}}_i$ are not collinear, and the particles undergo curved trajectories which either are interrupted by another collision (Fig. 1b) or converge to the straight stationary state (Fig. 1a).

In the following we will refer to *binary scattering events*, which must not be confused with the binary *collisions*: A binary scattering event starts at the time of a first collision, when both particles have speed v_0. After a number of re-collisions the particles escape each other, and the dynamics restores the speed of both particles to v_0. Only when these conditions are eventually met, the binary scattering event (or "scattering sequence") is over. We insist that while the momentum is conserved by the collisions themselves, the intrinsic self-propulsion dynamics enforces the particles to recover their steady velocity later, and thereby destroys momentum conservation. Note also that a single binary scattering event can comprise one or many collisions, depending on angle and lateral offset of the incoming particles.

2.4. Comparison with other models

Before starting the numerical study and theoretical analysis of the present model, it is of interest to compare it to other models of self-propelled disks found in the literature. As shown in [21], the proper tool to conduct such a comparison is to evaluate the change of momentum occurring during scattering events, in the sense defined above. Since, by definition the scattering event ends when $\mathbf{v}_i = \hat{\mathbf{n}}_i$, the only concern is to evaluate the impact of the collision on the body vectors $\hat{\mathbf{n}}_i$.

An interesting non-overdamped model of active colloids is that of soft active colloids [17], in which the dynamics of $\mathbf{v}$ is similar to Eq. (2), but the dynamics of $\hat{\mathbf{n}}$ is totally slaved to the one of $\mathbf{v}$. This is the limit $\tau_n \to 0$ in Eq. (3). Here the softness of the interaction potential introduces an interaction timescale τ_i: the softer the repulsion, the longer the interaction time, the more inelastic is the scattering. As such, comparing the outcome of the scattering events in both models, the ratio τ_i/τ_v for the soft colloids plays a similar role as our parameter α. It is then not surprising that the binary scattering of the soft active colloids and our above model share qualitatively the same features [17]. In view of our results presented below, one thus expects that the soft active colloids also display a discontinuous transition between the isotropic and the ordered phase in the homogeneous regime. Although the authors have not studied in detail the order of transition, their simulation data in the homogeneous regime are indeed compatible with a discontinuous transition in the dilute regime [17].

In other models motivated by migrating cells [16, 22], the orientation $\hat{\mathbf{n}}$ has richer dynamics and tends to align towards $\mathbf{v}$ on a timescale τ_n, as in Eq. (3). In this case the soft interaction again orients the velocities $\mathbf{v}_i$. The orientations $\hat{\mathbf{n}}_i$ follow on the timescale τ_n, but only during the interaction time τ_i, because of the overdamped dynamics. Again,

comparing the outcome of the scattering events in both models, it is thus here τ_n/τ_i which plays a role similar to that of our parameter α.

To our knowledge, the general case of a non-overdamped dynamics for the velocity, with soft interactions, and a dynamics for the orientation akin to the one proposed here and in [16, 22] has not been investigated yet. We infer from the above discussion that the dynamics would be very similar to the one described below: what matters is the persistence of the orientation $\hat{\mathbf{n}}$ across the scattering event.

As a matter of fact, the widely studied class of models found in the literature, and referred to as *active brownian particles* perfectly illustrates this last remark. In that case the dynamics of $\mathbf{v}$ is again overdamped while $\hat{\mathbf{n}}$ simply undergoes angular diffusion independent of $\mathbf{v}$. Here also the $\mathbf{f}_{ij}$ express soft repulsive interactions [23, 24]. This kind of models are strictly non-aligning because the dynamics has no memory of the interaction: in the absence of noise $\hat{\mathbf{n}}$ is infinitely persistent. From that point of view these models behave qualitatively like ours in the limit $\alpha \to \infty$: at the end of a binary scattering event, both velocities $\mathbf{v}$ relax towards their respective $\hat{\mathbf{n}}$ which keeps memory of the pre-scattering velocities.

3. Molecular dynamics simulations

We now establish the phase behaviour of the model for N particles. Molecular dynamics (MD) simulations were performed at $\tau_v = 4$ with $N = 1000$ or $N = 4000$, focusing on the dilute regime $\rho \ll 1$ (see below for a discussion of the effect of τ_v). We are thus left with two microscopic parameters, namely α and D/λ. Also, the system size is chosen not too large, in order to keep the system spatially homogeneous, which we have checked by visual inspection. We measured the order parameter $\psi(t) = \left|\sum_i \mathbf{v}_i(t)\right|/N$, which is of order $1/\sqrt{N}$ for the isotropic state and of order one for the polar state.

Let us first look at the case without angular noise, $D/\lambda = 0$. We initialized simulations from random isotropic conditions and waited for the isotropic state to eventually destabilize. When a stationary state was reached, we started to average the order parameter over time, $\langle\psi\rangle$. As shown in Fig. 1c, we found the isotropic state to be stable at low values of α, whereas it becomes unstable at larger values, in favour of a polar state. Between the two phases, an abrupt discontinuous transition takes place at α_*. Quite remarkably, in the whole polar phase the dynamics converges to $\psi = 1$, where particles are all strictly parallel. Further, choosing some random state with $\psi \approx 1$ as initial condition, we found that the polar state $\psi = 1$ is stable for all $\alpha > 0$, in particular also when $\alpha < \alpha_*$. In Fig. 2a, we show again the (now rescaled) order parameter in the isotropic state, this time for different densities. For a given density, the data for different values of N collapse, showing that finite-number effects are under control. In all cases we observed convergence to the fully polar state beyond the points shown. The theoretical framework used below adds the line for $\rho \to 0$, drawn in black. Increasing density here clearly favours the polar state. The departure of the transition due to density effects, $1 - \alpha_*(\rho)/\alpha_*(0)$, is plotted in Fig. 2b.

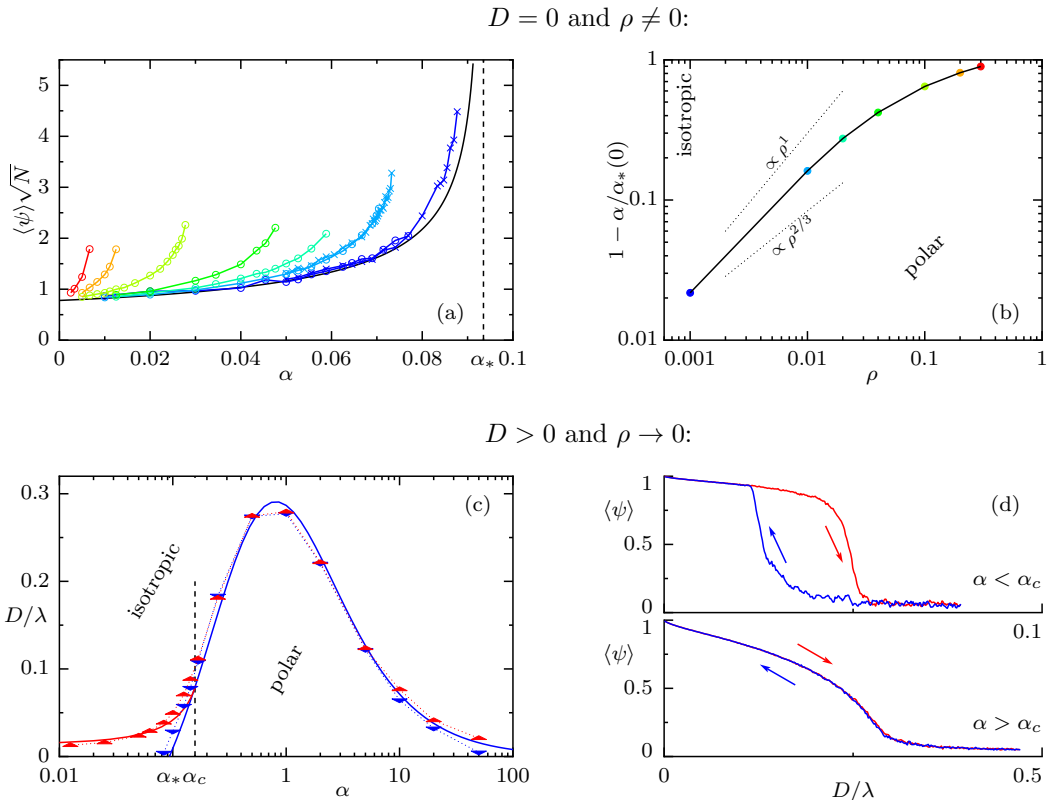

Figure 2. **(a)** Order parameter in the isotropic phase, without angular noise. $N = 1000$ (circles) and 4000 (crosses). From right to left: theory at $\rho \to 0$, $\rho = 10^{-3}$, 0.01, 0.02, 0.05, 0.1, 0.2, 0.3. **(b)** Dependence of the isotropic–polar transition on the density, with no angular noise. **(c)** Transition lines in the $(\alpha, D/\lambda)$-plane, at fixed density $\rho = 0.01$. Solid lines are theoretical results at $\tau_v = \infty$. Upward triangles (red) and downward triangles (blue) are transitions measured numerically by respectively increasing and decreasing D/λ quasi-statically. **(d)** Order parameter obtained by increasing (red) and decreasing (blue) the angular noise.

Adding angular noise to the trajectories quite changes the picture. During simulations we first increased D/λ quasi-statically and then decreased it again. The transition was measured by looking at the maximum of the fluctuations of the order parameter among many realizations of the dynamics. The resulting phase diagram at density $\rho = 10^{-2}$ is shown in Fig. 2c. In agreement with intuition,the isotropic state is always stable at strong enough angular noise. When decreasing the noise we pass into the polar phase, but the nature of this transition can be either discontinuous or continuous. For values $\alpha < \alpha_c \approx 0.157$ the transition has some hysteresis, as indicated in the upper panel of Fig. 2d. The discontinuous nature of the transition is thus robust when adding angular noise. There is coexistence in phase space of the isotropic and the polar homogeneous states. For $\alpha > \alpha_c$, the hysteresis is no longer observed at our level of numerical precision¶, as can be seen in the lower panel of Fig. 2d. At α_c, the coexistence

¶ In the last three points of Fig. 2c, for $\alpha \geq 10$ there is a slight hysteresis which disappears for slower annealing rate of D/λ.

zone vanishes into a single line of transition (tricritical point [25, 26, 27]). Interestingly, once in the polar phase, further increasing α leads to a re-entrant transition towards the isotropic phase.

4. Kinetic theory framework

We now rationalize these numerical observations in the context of kinetic theory, using the properties of the binary scattering, following Refs. [17, 21]. We summarize here the procedure described in Ref. [21]. In the dilute regime, the mean free-flight time λ^{-1} is long enough so that particles have mostly reached their stationary velocity v_0 before interacting with another particle ($\tau_v, \tau_n \ll \lambda^{-1}$). The binary scattering of self-propelled particles does not conserve momentum, and that is why a polar state can emerge from an isotropic initial condition. Assuming molecular chaos and choosing the von Mises distribution as an ansatz for the angular distribution of the velocities, one can write down an evolution equation for the order parameter ψ. This equation can then be expanded, up to order ψ^3 to study the stability of the isotropic phase [21]:

$$\frac{1}{\lambda}\frac{\mathrm{d}\psi}{\mathrm{d}t} \simeq \big(\mu - D/\lambda\big)\psi - \xi\psi^3, \tag{6}$$

where the coefficients are given by

$$\mu := \big\langle \mathbf{p}\cdot\delta\mathbf{p}\big\rangle_0, \tag{7}$$

$$\xi := \big\langle (\tfrac{1}{2} - \cos\Delta)\,\mathbf{p}\cdot\delta\mathbf{p}\big\rangle_0, \tag{8}$$

$$\langle f\rangle_0 := \frac{1}{4}\int_{-1}^{1}\mathrm{d}b\int_0^{\pi}\mathrm{d}\Delta\,\Big|\sin\frac{\Delta}{2}\Big| f(b,\Delta). \tag{9}$$

In the stationary state, the left-hand size of Eq. (6) vanishes. The transition line is obtained by solving the equation $\mu(\alpha_*) = D/\lambda$ for α_*, while the sign of $\xi(\alpha_*)$ at the transition tells whether it is continuous or discontinuous. The coefficient μ is exact within the assumptions of kinetic theory, while ξ should depend on the ansatz used for the angular distribution. Both coefficients are an average over all pre-scattering parameters, as given in Eq. (9), where b is the impact parameter and Δ is the angle between the incoming particles' velocities. The averaging needs not be done over the norms of the velocities, since those are fixed to $v_0 = 1$. We have checked explicitly that this assumption holds very well in the numerical simulations in the dilute regime. In Eqs. (7) and (8), $\mathbf{p}$ is the pre-scattering momentum of the two colliding particles, and $\delta\mathbf{p}$ is the change of their momentum by the scattering event. In contrast with Ref. [17], the above equations explicitly identify the *forward component of the momentum change* $\mathbf{p}\cdot\delta\mathbf{p}$, as the proper quantity to describe the alignment in a binary scattering event. The predictions thus depend only on the microscopic details of the deterministic dynamics through the scattering function $\mathbf{p}\cdot\delta\mathbf{p}(b,\Delta)$, which we now explore for the model (1)–(3).

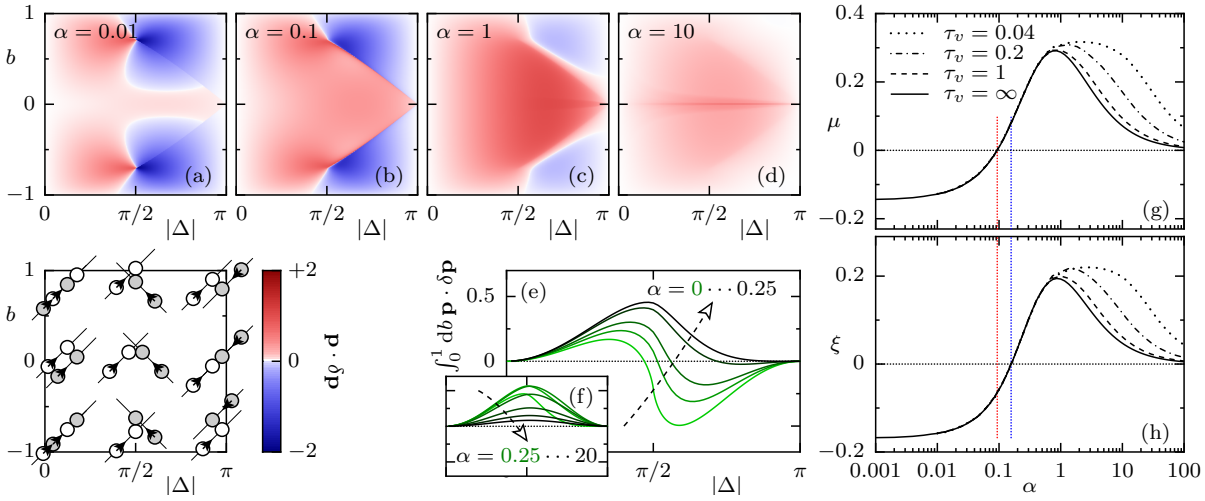

Figure 3. Top: Colour maps of the full scattering function $\mathbf{p} \cdot \delta\mathbf{p}(b, \Delta)$. The geometry of the collisions and the colour scale are shown in the bottom-left panel. **Bottom–middle:** the partially integrated scattering function as a function of the incoming angle Δ, for different values α, $\tau_v = 4$. **Right:** Fully integrated scattering functions μ and ξ, defined in Eqs. (7) and (8) plotted as a function of α for different τ_v. The red vertical line indicates α_*, the transition in the absence of noise. The blue vertical line indicates α_c.

5. Binary scattering

Remind that a scattering event can consist of several, if not many, hard-disk collisions, such as depicted in Fig. 1b. Before the first collision, both particles are taken to be in the stationary state, i.e. $\mathbf{v} = \hat{\mathbf{n}}$. After the collision, we integrate Eqs. (1)–(3) numerically until another collision possibly occurs. The binary scattering is considered over when both particles have again reached their stationary state and are heading away from each other. Repeating the procedure in the whole range of initial parameters (b, Δ) yields the scattering function $\mathbf{p} \cdot \delta\mathbf{p}(b, \Delta)$. Figure 3 shows this function for several α, as well as its integral over b and the full integrals yielding the coefficients μ and ξ.

Let us stress that $\mathbf{p} \cdot \delta\mathbf{p}$ is not changed by the collision itself, which conserves momentum. All (dis)alignment must here come from the relaxation of the post-collisional value of $|\mathbf{v}|$ to unity. Fig. 3a–d shows that scattering at low angular separation, small Δ, always creates forward momentum. In other words, two nearly parallel particles that interact become even more parallel, which gives rise to an effective alignment, $\mathbf{p} \cdot \delta\mathbf{p} > 0$. On the other hand, for small enough α, particles that enter in interaction frontally ($\Delta \approx \pi$) tend to disalign, except for special symmetry such as $b \approx 0$. Increasing α favours aligning scattering events until eventually only aligning events remain. This is best summarized by integrating out all parameter dependence except the incoming angle, as is plotted in Fig. 3e,f.

The coefficients μ and ξ are then obtained by integrating over Δ, with weights prescribed by Eqs. (7) and (8). Their dependences on the microscopic parameters of the dynamics, α and τ_v, are shown in Fig. 3g,h. In the absence of noise, the transition

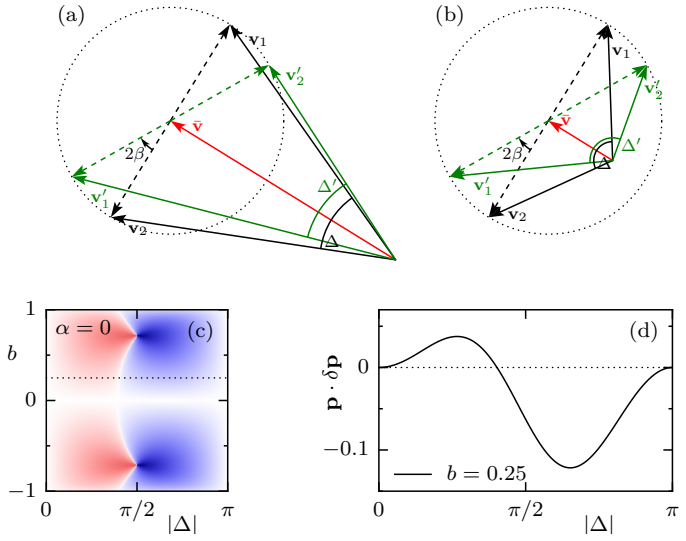

Figure 4. **(a,b)** Elastic collisions are rotations by an angle $2\beta = 2\mathrm{asin}(b)$ in the reference frame of the center-of-mass velocity $\bar{\mathbf{v}}$. Primed quantities (green) are post-collisional, black ones are pre-collisional. **(c)** The scattering function $\mathbf{p}\cdot\delta\mathbf{p}$ resulting from a single collision. **(d)** A cut through (c) along the dotted line, for the value of b used in (a,b).

occurs for $\alpha = \alpha_*$ such that $\mu(\alpha_*) = 0$; $\xi(\alpha_*)$ is negative, hence the discontinuous transition. When angular noise is added, the transition is obtained by solving the equation $\mu(\alpha_*) = D/\lambda$. From the shape of the curve $\mu(\alpha)$, one obtains two values $\alpha_\pm$, with $\alpha_- \to \alpha_*$ and $\alpha_+ \to \infty$ when $D \to 0$. As D/λ is increased, $\xi(\alpha_-)$ eventually becomes positive and the transition turns continuous at a tricritical point $(\alpha_c, D_c/\lambda)$. Note that $\xi(\alpha_+) > 0$: the re-entrant transition is always continuous. Regarding the role of τ_v, α_- is practically independant on τ_v, while α_+ increases when τ_v decreases. The theoretical predictions are shown as solid lines in Fig. 2c. The agreement with the MD simulations data for density $\rho = 10^{-2}$ is excellent. The small shift of the measured transition lines to the left with respect to the theoretical one comes from finite-density effects.

Finally, we also learn from the examination of the scattering maps that, in the absence of noise, the polar phase $\psi = 1$ is actually an absorbing phase [28]: this is because *all* binary scattering events at small Δ have $\mathbf{p}\cdot\delta\mathbf{p} > 0$. When all particles in a system are sufficiently parallel, binary scattering events can only align the system more. This is true for all α, and most remarkably for $\alpha \to 0$.

Altogether, our kinetic theory description, using the von Mises ansatz for the angular distribution, captures quantitatively all the phenomenology reported in the numerical simulations at low enough density. It however relies on the numerical evaluation of the scattering maps. In the last part of the paper, we would like to provide some intuition on the origin of the peculiar form of these maps. Also, we will elucidate the role of the multiple collisions which can take place during a scattering event.

6. Analytical limits

When we take the limit $\tau_n \to 0$, the vector $\hat{\mathbf{n}}$ has no persistence at all. After two particles collide elastically, the $\hat{\mathbf{n}}$ rotate to their respective $\mathbf{v}$ instantaneously, the two particles cannot collide a second time and the post-collisional relaxation of $|\mathbf{v}|$ to unity occurs on a straight trajectory. We take advantage of this simplification to compute the scattering map in the case $\alpha = 0$. Because velocities have equal modulus, we can use the nice visualisation of an elastic collision as a rotation in the center-of-mass frame (Fig. 4a,b). One can then find an analytic expression[+] for $\mathbf{p} \cdot \delta\mathbf{p}(b, \Delta)$, which is plotted in Fig. 4c. This plot nicely completes the series of varying α from Fig. 3a-d. The essential structure of the scattering maps can be accounted for by the sole ingredients present in the case $\alpha = 0$. Inelastic collisions and persistence of $\hat{\mathbf{n}}$ are not essential. Conversely, non-conservation of momentum due to the relaxation of the particle speeds to unity is crucial.

At values $\alpha > 0$, the vector $\hat{\mathbf{n}}$ has non-vanishing persistence, which results in curved trajectories and possible recollisions. This could lead to the effective alignment mechanism which was proposed to be at the root of the collective motion in the experiment of vibrated polar disks [18, 19, 20]. Concerning the influence of recollisions in the scattering, we ask whether they contribute significantly to μ and ξ. In particular, how numerous are they depending on the scattering geometry (b, Δ), what is their statistical weight and how much do they affect the scattering map $\mathbf{p} \cdot \delta\mathbf{p}(b, \Delta)$? One can get an intuitive picture of the recollision mechanism looking at a simple case, the symmetric ($b = 0$) binary scatterings in Fig. 5a. A first collision makes $\mathbf{v}$ rotate from being equal to $\hat{\mathbf{n}}$ to pointing away from the other particle. On the following trajectory, $\mathbf{v}$ and $\hat{\mathbf{n}}$ relax towards each other, on their respective timescales τ_v and τ_n. For small enough τ_v, the persistence of $\hat{\mathbf{n}}$ allows for a recollision to take place, and both vectors get closer to each other from one collision to the next. The highly symmetric case depicted in Fig. 5a is however so degenerate that it has either one or infinite collisions*. Unfortunately, the analytic treatment of asymmetric collisions is much too technical to gain physical insight from it and we prefer coming back to the numerical sampling of the scattering events.

For $\alpha = \alpha_-$, as shown in Fig. 5b (top row), recollisions can be numerous, but take place only in a small region of the parameter space (b, Δ), the smaller the larger τ_v. We measure their relative contribution to $\mathbf{p} \cdot \delta\mathbf{p}$ by $\Upsilon = \frac{1}{2}\sin(\Delta/2)(\mathbf{p} \cdot \delta\mathbf{p} - \mathbf{p} \cdot \delta\mathbf{p}|_1)/|\mathbf{p} \cdot \delta\mathbf{p}|$, where $\mathbf{p} \cdot \delta\mathbf{p}|_1$ is the contribution of the first collision only. As shown in Fig. 5b (bottom row), even for the smallest value $\tau_v = 0.04$, this contribution is locally less than 5 %. For larger τ_v, the contribution is vanishingly smaller. Thus, recollisions

[+] $\mathbf{p} \cdot \delta\mathbf{p}(b, \Delta) = 2\cos\frac{\Delta}{2} \sum_{s=-1,1} \left[\frac{\cos\frac{\Delta}{2} + 2sb\sqrt{1-b^2}\sin\frac{\Delta}{2}}{\sqrt{1+2sb\sqrt{1-b^2}\sin\Delta}} - \cos\frac{\Delta}{2} \right]$

* In the symmetric case, linearizing the dynamics around the stationary point provides analytical results about this mapping from one collision to the next. For $\alpha < 1$, there is no recollision. For $\alpha > 1$, an infinite number of recollisions occur, with a collision rate that converges to a positive constant ($\alpha < 2$) or diverges ($\alpha > 2$).

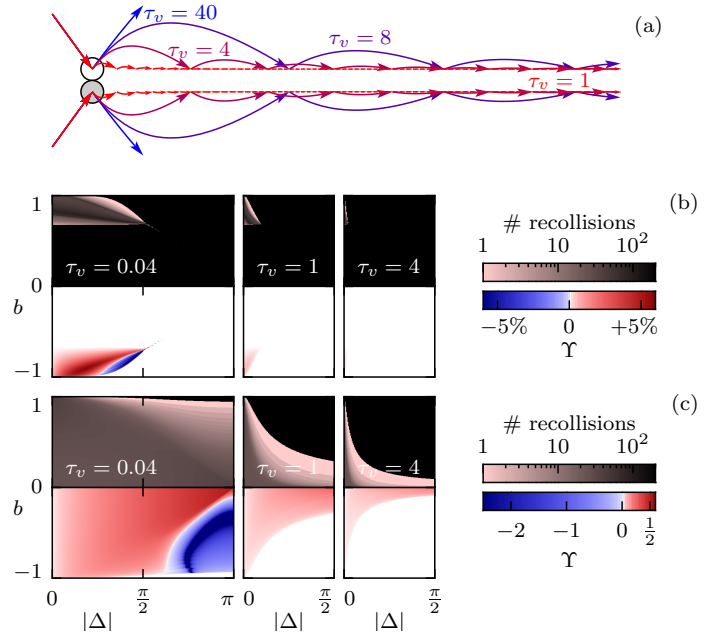

Figure 5. Recollisions. **(a)** Symmetric binary scatterings for $\alpha = 5$. **(b, c)** Number of recollisions in each scattering (top rows) and their relative contribution to $\mathbf{p} \cdot \delta\mathbf{p}$ (bottom rows). $\alpha = 0.1$ for (b), $\alpha = 10$ for (c).

has no practical influence on the transition at $\alpha = \alpha_-$. Conversely, as shown in Fig. 5c (top row), for $\alpha = \alpha_+$, the number of recollisions is not so large, but they occur for wider ranges of scattering parameters and their relative contribution to $\mathbf{p} \cdot \delta\mathbf{p}$ is significant, see Fig. 5c (bottom row). This is all the more true for smaller τ_v and is responsible for the dependance of μ and ξ on τ_v in this regime.

7. Discussion

Let us recast our main findings and the understanding we obtained from the above analysis. A homogeneous system of self propelled hard disks, obeying the minimal deterministic Eqs. (1)–(3), exhibits a sharp discontinuous transition from an isotropic to an absorbing polar collective motion state, when increasing the persistence of the body axis vector $\hat{\mathbf{n}}$. Adding angular noise, the transition becomes continuous via a tricritical point. At fixed noise level, increasing further the persistence of the body axis vector, a re-entrant continuous transition from the polar state to the isotropic state occurs.

All these macroscopic behaviours can be understood by the study of the scattering maps $\mathbf{p} \cdot \delta\mathbf{p}$, which describe the level of alignment of all possible scattering events. The most striking feature of these maps is that scattering at low angular separation always creates forward momentum. This is even true for $\alpha = 0$, for which, we could prove it explicitly from a mechanical analysis of the collisions. This feature explains the stability of the polar phase in the absence of noise. For small α, the dis-alignment, present in

the frontal collisions is strong enough to stabilize the isotropic state. For $\alpha > \alpha_*$, this does not hold anymore, and the isotropic state becomes unstable. The coexistence of stability of the two states for $\alpha < \alpha_*$ guarantees the transition to be discontinuous.

The effect of noise is most easily understood from the shape of the curves $\mu(\alpha)$ and $\xi(\alpha)$. The key point here is that in the present scheme of approximation – Boltzmann equation plus von Mises Ansatz – the computation of ξ is identical to that of μ, apart from the additional asymmetric factor $(1/2 - \cos\Delta)$. This does not rely on the specificity of the microscopic model. As a result, the curve $\xi(\alpha)$ is similar to the curve $\mu(\alpha)$, with a shift towards larger α. Adding noise simply shifts the transition towards larger α: at some point ξ changes signs at the transition, which becomes continuous, hence the tricritical point.

Finally, the re-entrant transition from polar back to isotropic at large α (while increasing α) is a direct consequence of the non-monotonous shape of $\mu(\alpha)$. At moderate α, the effective alignment μ increases with the persistence of $\hat{\mathbf{n}}$. However, a too large persistence reduces the alignment, because the scattering event does not reorient $\hat{\mathbf{n}}$ significantly, and no memory of the collision is kept: $\mathbf{v}$ relaxes to practically the same $\hat{\mathbf{n}}$ as before the scattering. Some alignment still takes place but is most easily destroyed by small amounts of noise. Interestingly, while the recollisions play no role at the first transition from the isotropic to the polar state, they here increase the effective alignement and thereby postpone the re-entrant transition to larger α.

As can be seen from the above discussion, the results do not depend on the details of the scattering maps, as long as binary scattering at low angles produces effective alignment. The partially integrated scattering function (Fig. 3e,f) is then positive for small angles. Models which fall into this class are (i) the here described hard disks with mutual coupling between $\mathbf{v}$ and $\hat{\mathbf{n}}$, (ii) the inelastically colliding hard disks studied in [21] for which $\hat{\mathbf{n}} = \mathbf{v}$, and (iii) the soft disks described in Ref. [17]. As already partly discussed in the introduction, it is quite clear now that introducing softness or inelasticity to the model studied here, it would still remain in the same class of models.

It is important to note that the distinctive behavior of the above class of systems is markedly different from the original Vicsek model, in which binary scattering at low angle effectively disaligns. In the Vicsek model, the partially integrated scattering function (Fig. 2a of Ref. [21]) behaves precisely in the opposite way of the one here (Fig. 3e). It is therefore unlikely that a coarse-graining of self-propelled hard disks (or any of the above three models) would yield the Vicsek model. It would be very interesting to know what might be the impact of the order of the mean-field transition in the case of large system sizes, when spatial heterogeneities are prone to take place. Preliminary simulations as well as the results already present in [20] indicate that localized band-like structures indeed appear for large and dense enough systems. However, whether those structures are truly identical to the ones obtained in the simulations of the Vicsek model or from the analysis of the long wavelength hydrodynamics equations [29, 30], is a completely open issue. One possible step towards a better understanding of this regime would consist in taking the Landau terms to 5th

order, with a destabilizing cubic term and a saturating 5th order term. In principle, the coexistence of the two homogeneous solutions in phase space, and the plausibly absorbing character of the polar state, could lead to complex spatio-temporal dynamics, such as those observed in the so-called subcritical turbulence [31, 32].

Altogether, the present new class of models, including the self-propelled hard particles, could well play for the theory of "simple active liquids" the role that hard spheres play for the statistical mechanics of gases.

[1] Vicsek T, Czirók A, Ben-Jacob E, Cohen I and Shochet O 1995 *Phys. Rev. Lett.* **75**(6) 1226–1229
[2] Toner J and Tu Y 1995 *Phys. Rev. Lett.* **75** 4326–4329
[3] Bertin E, Droz M and Grégoire G 2006 *Phys. Rev. E* **74** 22101
[4] Chaté H, Ginelli F, Grégoire G and Raynaud F 2008 *Phys. Rev. E* **77**(4) 046113
[5] Ihle T 2011 *Phys. Rev. E* **83** 030901
[6] Peshkov A, Bertin E, Ginelli F and Chaté H 2014 *Eur. Phys. J. Special Topics* **223** 1315–1344
[7] Zhang H P, Be'er A, Smith R S, Florin E L and Swinney H L 2009 *EPL (Europhysics Letters)* **87** 48011
[8] Zhang H P, Be'er A, Florin E L and Swinney H L 2010 *Proceedings of the National Academy of Sciences of the United States of America* **107** 13626–13630 URL `http://dx.doi.org/10.1073/pnas.1001651107`
[9] Chen X, Dong X, Be'er A, Swinney H L and Zhang H P 2012 *Phys. Rev. Lett.* **108** 148101
[10] Schaller V, Weber C, Semmrich C, Frey E and Bausch A R 2010 *Nature* **467** 73–77
[11] Peruani F, Deutsch A and Bär M 2006 *Phys. Rev. E* **74** 30904
[12] Baskaran A and Marchetti M C 2008 *Phys. Rev. E* **77** 011920 URL `http://dx.doi.org/10.1103/PhysRevE.77.011920`
[13] Ginelli F, Peruani F, Bär M and Chaté H 2010 *Phys. Rev. Lett.* **104** 184502 URL `http://dx.doi.org/10.1103/PhysRevLett.104.184502`
[14] Aranson I S and Tsimring L S 2005 *Phys. Rev. E* **71** 050901
[15] Grossman D, Aranson I S and Ben-Jacob E 2008 *New Journal of Physics* **10** 023036
[16] Henkes S, Fily Y and Marchetti M C 2011 *Phys. Rev. E* **84** 040301(R)
[17] Hanke T, Weber C A and Frey E 2013 *Phys. Rev. E* **88**(5) 052309
[18] Deseigne J, Dauchot O and Chaté H 2010 *Phys. Rev. Lett.* **105** 098001
[19] Deseigne J, Léonard S, Dauchot O and Chaté H 2012 *Soft Matter* **8** 5629–5639
[20] Weber C A, Hanke T, Deseigne J, Léonard S, Dauchot O, Frey E and Chaté H 2013 *Phys. Rev. Lett.* **110**(20) 208001
[21] Nguyen Thu Lam K D, Schindler M and Dauchot O 2015 *J. Stat. Mech.* in press arXiv:1410.4520
[22] Szabó B, Szöllösi G J, Gönci B, Jurányi Z, Selmeczi D and Vicsek T 2006 *Phys. Rev. E* **74** 061908
[23] Romanczuk P, Bär M, Ebeling W, Lindner B and Schimansky-Geier L 2012 *European Physical Journal Special Topics* **202** 1–162
[24] Fily Y and Marchetti M C 2012 *Physical Review Letters* **108** 235702
[25] Chaikin P M and Lubensky T C 1995 *Principles of condensed matter physics* (Cambride, U.K.: Cambride University Press)
[26] Baglietto G, Albano E V and Candia J 2013 *Physica A* **392** 3240–3247
[27] Romenskyy M, Lobaskin V and Ihle T 2014 *arXiv:1406.6921*
[28] Hinrichsen H 2000 *Adv. Phys.* **49** 815–958
[29] Caussin J B, Solon A, Peshkov A, Chaté H, Dauxois T, Tailleur J, Vitelli V and Bartolo D 2014 *PRL* **112** 148102
[30] Solon A P, Chaté H and Tailleur J 2015 *Phys. Rev. Lett.* **114** 068101
[31] Manneville P and Dauchot O 2001 Patterning and Transition to Turbulence in Subcritical Systems: The Case of Plane Couette Flow *Coherent Structures in Complex Systems* (Berlin, Heidelberg: Springer Berlin Heidelberg) pp 58–79 ISBN 978-3-540-41705-7

[32] Prigent A, Grégoire G, Chaté H, Dauchot O and van Saarloos W 2002 *PRL* **89** 014501–4